

# Energy and strength in brittle materials

Emanuela Speranzini\*

Department of Engineering, University of Perugia, via G. Duranti n.93, 06125 Perugia, Italy

(Received February 28, 2019, Revised March 8, 2019, Accepted March 10, 2019)

**Abstract.** A study concerning the strength of brittle materials is presented in this paper. The failure behavior was investigated examining the plane of the crack after the failure and comparing the results obtained with those deriving from the fracture mechanics theory. Although the proposed methods are valid in general for brittle materials, the experiment was performed on glass because the results are more significant for this. Glass elements of various sizes and different edge finishes were subjected to bending tests until collapsing. The bending results were studied in terms of failure load and energy dissipation, and the fracture surfaces were examined by means of microscopic analysis, in which the depth of the flaw and the mirror radius of the fracture were measured and the strength was calculated. These results agreed with those obtained from the fracture mechanics analysis.

**Keywords:** brittle material; energy; strength; structural glass; ceramic

## 1. Introduction

There is generally a certain stress threshold in the mechanical behavior of all materials, beyond which the elastic behavior is lost. In brittle materials this threshold is considered to be a breaking point, whereas in ductile materials the loss of elastic behavior represents the yield point, beyond which there are additional resources that change its constitutive law.

The weakness of brittle materials derives from the presence of microscopic surface and/or volume defects, which can propagate and evolve into macroscopic fractures, until the structural element collapses (Foraboschi 2009, 2017). Depending on many factors such as size and shape of surface defects, close flaws may interact with one another, evolving into a multiple fracture Castori and Speranzini (2017). Therefore, in order to understand the mechanical behavior of brittle materials, it is necessary to be able to predict and control the development of their defects, which depends not only on stress but also on physical and chemical interactions with the environment. Strength depends on the size of the greater defect which is called the critical defect.

A large amount of research has been conducted on brittle materials concerning different response to tensile and compressive (Brencich *et al.* 2001), cracking of quasi brittle materials under monotonic and cyclic loadings (Cervera *et al.* 2018), performances of pantographic structures affected by statistically distributed defects (Turco *et al.* 2016) and multiple crack evaluation on concrete using a line laser thermography scanning system (Jang and An 2018, Surkay *et al.* 2018, Kim and Cho 2018).

Research on the strength of brittle materials as function of defects goes back into the past and was mainly concerned with glass and ceramic materials (Wiederhorn and Evans (1974). These materials are subject to stress-corrosion, a complex phenomenon still under investigation, which causes defects to evolve under constant external stress even well below the theoretical strength limit. This circumstance attracted considerable interest, as can be seen from the impressive amount of published works on this topic, among which are the studies by Charler (1958), Wiederhorn (1970). A review on this topic has been written by Ciccotti (2009). Like all the other material corrosions, glass stress-corrosion is governed by a set of physical and chemical phenomena occurring at the micro/nanoscale, whose main factors are the chemical composition of glass, the presence of water or water vapour in the atmosphere, the temperature of the environment and the pH (Briccoli *et al.* 2010, Andreozzi *et al.* 2015). This phenomenon is caused by the growth of small cracks in the surface and the combination of the influence of humidity and the applied loads. Another problematic feature of brittle nonmetallic materials is the size effect i.e., the decrease in the strength due to the increase in the size of the structural element (in volume or surface).

Studies on the behavior of materials affected by defects have been developed with the LEFM (Linear Elastic Fracture Mechanics) theory, in which the behavior of the material is modeled by looking at cracks (Carpinteri 1992). Given that glass is an elastic-brittle material, it was used for developing the basics of this theory. A stress analysis conducted on an elliptical cavity in a uniformly stressed plate showed that the local stress surrounding a notch or corner could rise to a level several times higher than the applied stress, and then even submicroscopic flaws might be potential sources of weakness in materials.

Fracture surface analysis can provide useful suggestions for the study of brittle materials. Different types of crack

---

\*Corresponding author, Professor  
E-mail: [emanuela.speranzini@unipg.it](mailto:emanuela.speranzini@unipg.it)

growth (e.g., fatigue, stress corrosion cracking, and excessive loading) produce characteristic features on the surface that can be used to help identify the failure mode (Castilone *et al.* 2002). One of the aims of fractographic inspection is to determine the cause of failure and calculate the failure strength by means of certain physical parameters, such as the depth of the flaw and the mirror radius of the fracture, which are measured after the failure of the material (Marsili *et al.* 2017). It can also be used in a more fundamental manner to develop and evaluate theoretical models of crack growth behavior. This technique has been widely used for brittle materials such as glassy carbon, ceramics and glass. *Glassy carbon* is a brittle form of carbon with a randomized structure and offers high purity, corrosion resistance, thermal stability and a structure impermeable to both gases and liquids. It is used in vessels for ultra-high purity materials technology, semiconductor connections and protective tubes for heating elements. *Ceramic materials* are used in bioengineering for prosthesis, and in the automotive and aerospace industries for their higher fracture toughness and resistance to high temperatures, while *advanced ceramic materials* are especially suitable for corrosive environments and are widely used in the aeronautics and aerospace sectors. *Glass-ceramic* is attractive for its high abrasion and chemical resistance, is used in the building industry, and is also a promising material for structural uses (Collini and Royer 2014).

This paper investigated the failure behavior of the brittle materials examining the plane of the crack after the failure. In this investigation it was decided to use specimens of annealed float glass because the results were expected to be more significant than with other brittle materials, due to glass transparency. Rectangular glass elements were cut from a sheet of glass and the edges were ground and/or left simply cut. These were loaded to bending in the plane, and the corresponding results were studied in terms of strength and energy dissipation. The fracture surface was analyzed by using microscopic analysis. The results obtained are in agreement with those obtained from the linear elastic fracture mechanics theory. This survey proves the possibility of determining the stress of brittle materials at the time of breaking directly on the fragments by means of analyses and measurements performed on the plane containing the fracture surface. This approach can be used for investigations after breakage and to validate the theoretical results of new studies concerning brittle structures.

## 2. Methods

### 2.1 The theory of brittle materials failure

Defects in the materials are to be considered the main causes of triggering brittle fractures; this is why a theory for the study of cracks has been developed. A crack is an idealized model of a flaw with a defined geometry and lying in a plane, located on the surface or embedded within the volume. The effects of the stress concentration in the

vicinity of flaws and defects have been studied since the late 1800s, when Kirsch investigated the problem of a glass pane with a round hole and subjected to traction, and then Inglis (1913) extended the study to the more general case of a glass sheet with an elliptical hole, in which the strength of the material depends on the ratio between the axes of the hole's ellipse. In 1920 Griffith, in analyzing the fracture phenomenon, referred to energy considerations in addition to stress and showed that the elastic strain energy  $U_E$  released by a glass pane of unitary thickness, subjected to traction  $\sigma$ , when this is cut with an incision having a length of "2a" and the displacements without end are kept constant, is proportional to the energy contained in the circle with radius  $a$  before the incision. Griffith added that to create a cut of length  $2a$  it is necessary to have a surface energy  $U_S$  required by the new portion of open surface created. Therefore  $U_E$  and  $U_S$  are expressed in

$$U_E = \frac{\pi a^2 \sigma^2}{E} \quad (1)$$

$$U_S = 4a\gamma$$

where  $E$  is the elastic modulus of the material and  $\gamma$  the energy related to the surface unit. Because a crack becomes unstable when the variation in strain energy resulting from an increase  $da$  in crack growth is sufficient to overcome the surface energy  $\gamma$ , the instability condition provides

$$\frac{\partial U_E}{\partial a} \geq \frac{\partial U_S}{\partial a} \quad (2)$$

$$\sigma_F = \sqrt{\frac{2\gamma E}{\pi a}}$$

where  $\sigma_F$  is the failure stress of the material. If there is  $\sigma < \sigma_F$ , the crack is stable and does not propagate; on the contrary, with  $\sigma > \sigma_F$  the fracture propagates spontaneously.

Irwin (1957) introduced the concept of the stress intensity factor (SIF)  $K_I$ , expressed to evaluate structural element failure. The general relationship among  $K_I$ , the nominal tensile stress normal to the crack's plane  $\sigma_n$ , the correction factor  $Y$  depending on the geometry of the crack and  $a$  representing the half-length of the crack (or defects), is given by

$$K_I = Y \sigma_n \sqrt{\pi a} \quad (3)$$

Eq. (3) is only valid in testing conditions where stress corrosion can be neglected. Otherwise, under loading and in humidity conditions, the subcritical crack growth propagates as a function of loading duration. In this condition the crack growth velocity is a function of the stress intensity factor  $K_I$  and of the environmental conditions.  $K_I$  falls between two limit values: the lower value  $K_{I0}$ , which depends on the environmental conditions, below which there is no propagation; and the upper critical value,  $K_{IC}$ , characteristic of the material, above which growth is independent of the environmental conditions and occurs at such speeds as to bring about instantaneous failure (for soda lime silica glass, for example, it is about 1500 m/s). The intermediate values of  $K_I$  define the sub-critical

growth interval of the fracture, which leads to delayed failure over time. Wiederhorn (1969) provided the following kinematic relationship between velocity  $v$  and the stress intensity factor  $K_I$

$$v = \frac{da}{dt} = v_0 \left( \frac{K_I}{K_{Ic}} \right)^n, \quad (4)$$

where  $v_0$  [m/s] represents the conventional value of the subcritical propagation of the crack, as it expresses the growth speed that the fracture would reach if it propagated up to the  $K_{Ic}$  following Eq. (4). Both  $v_0$  and  $n$  are constants that depend on the material and the environment, and they are measured by means of dynamic fatigue tests i.e. breaking tests in an aggressive environment at different loading speeds. In the case of glass, the values of  $v_0$  and  $n$  parameters are discussed by Haldimann (2006). The speed  $v_0$  can range from 30  $\mu\text{m/s}$  (relative humidity 0.2%) to 0,02 m/s in water and can be assumed equal to 0.01 mm/s in laboratory conditions and 6 mm/s in environmental condition. In order to achieve safety, the values of 0.0025 [m/s] can be assumed for  $v_0$  and 16 for  $n$  (relative humidity 100%), in any conditions.

Assuming Eq. (4), using the stress intensity factor from Eq. (3) and supposing  $n$  to be constant, it is possible to obtain the time-dependent size of a single crack subjected to the crack opening stress  $\sigma(t)$  as

$$a(t) = \left( a_i^{\frac{2-n}{n}} + \frac{2-n}{n} v_0 K_{Ic}^n (Y\sqrt{\pi})^n \int_0^t \sigma(\tau) d\tau \right)^{\frac{2-n}{n}}. \quad (5)$$

where  $a_i$  is the initial crack depth i.e.  $a_i = a(t=0)$ .

The same relation can be expressed in terms of the value  $\sigma$  with a static loading duration. It is possible to obtain the failure stress  $\sigma_f$ , knowing the failure loading duration  $t_f$  (s) and assuming  $a_{ci}$  (m) corresponding to the initial critical flaw depth

$$\sigma_f(t_f) = \left( \frac{2}{t_f(n-2)v_0(Y\sqrt{\pi}/K_{Ic})^n a_{ci}^{\frac{n-2}{n}}} \right)^{\frac{1}{n}}. \quad (6)$$

For a short duration of the applied loads, the *inert strength* (i.e. the failure stress that represents the strength in a crack when no subcritical crack growth occurs) regulates structure failure, whereas with increases in the loading duration, when stress corrosion phenomenon occurs, Eq. (6) is used to determine the failure stress, hereinafter called the strength. The theoretical transition loading duration, between the inert condition and time-dependent condition, expressed by the parameter  $t_{ref}$ , can be determined from Eq. (7) which is obtained using Eqs. (3) and (6). If  $t > t_{ref}$ , the strength decreases following Eq. (6); if instead  $t < t_{ref}$ , the

failure is assumed to follow the inert strength level.

$$t_{ref} = \frac{2a}{(n-2)v_0}. \quad (7)$$

### 2.2 Fracture surface analysis

The fracture surface is an important source of information for studying structural element failure. In this regard, the fractographic examination can be used in fractured elements of brittle materials, obtaining quantitative information about the loading condition at failure and the fracture origin, i.e. the sources from which the brittle fracture begins. In general, this origin can be traced to irregularities and defects in the material, such as pores and microcracks which occur due to manufacturing. Fracture analysis is a powerful tool for the interpretation of fractures of brittle solids.

Three different zones can be recognized around a crack on the fracture plane of the failure element: mirror, mist and hackle zones, along with crack branching shown in the Fig. 1, which represents an image of the typical fracture pattern centered around a surface flaw. The *mirror zone* forms around the critical flaw at the cross-section of the failed specimen. It is a relatively smooth region around the origin point. In glass this surface is highly reflective. The initial flaw may grow stably up to size  $a_c$  prior to unstable fracture, when the stress intensity reaches the value  $K_{Ic}$ . This region is characterized by a slow crack growth velocity and its size is inversely proportional to the square of the stress at fracture. In fact, under a failure stress, once the critical flaw starts to propagate, mirror boundary hackle lines are created after the radiating crack reaches terminal velocity. The mirror-mist radius is  $r_m$ . The *mist zone* is a flat smooth area surrounding the mirror region that shows a slight change in surface texture and is a transition zone from slow to fast crack growth. The mist-hackle radius is  $r_h$ . The outermost area, also called the *deformation zone*, includes hackles, striations and beach marks, and the texture of this area is directly related to the type of loading and the applied stress.

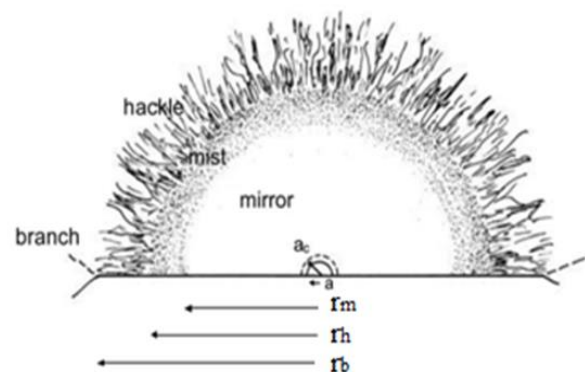


Fig. 1 Image of a typical fracture mirror centered on a surface flaw

The analysis of this region is critical for determining the causes of failure. The branching distance from the origin is  $r_b$ . The area of “a” radius is defined as the source of failure.

The three zones are easily identifiable in glass; it is more difficult, however, in ceramic because there is an inherent roughness from the microstructure also in the area immediately surrounding the origin. In coarse-grained or porous ceramics, it may be difficult to identify a mirror boundary. In polycrystalline ceramics, a mirror-mist boundary cannot be easily detected, due to the inherent roughness created by the crack-microstructure interactions also within the mirror.

A study of fracture patterns was presented by Quinn *et al.* (1990), in which the fracture surface can identify the cause and the origin of the failure. It also can determine whether a material contains unusual flaws or if the glass was simply overloaded. It was extensively demonstrated (Johnson and Holloway 1966, Levengood 1958) that the failure stress  $\sigma_f$ , i.e. the maximum principal tensile stress at the fracture origin, is proportional to the reciprocal of the square root of the mirror radius (radius of the mirror/ mist boundary)  $r_m$

$$\sigma_f r_m^{1/2} = B, \quad (8)$$

where  $B$  is a fracture mirror constant ( $\text{MPa m}^{1/2}$ ) that depends on the material properties. Similar relations were demonstrated in soda-lime glass for radii determined by the onset of hackle  $r_h$  and of crack branching  $r_b$  (Congleton and Petch 1967). Eq. (8) is considered valid in general for  $r_m$ ,  $r_h$ , and  $r_b$  to which correspond the fracture constants  $c_m$ ,  $c_h$  and  $c_b$ . However, limited information is available about the time-dependency of glass strength in relation to the mirror radius. The time-dependency in glass strength is not taken into consideration in the measurement of the mirror radius.

Fracture mirrors reveal fractographic markings that surround a fracture origin in brittle materials. The fracture mirror size may be used to estimate the stress in a fractured component when the fracture mirror constants are known or, alternatively, the fracture mirror size may be used in conjunction with known stress in test specimens to calculate fracture mirror constants.

Some studies have been carried out on the relationship between the speed of crack branching and fracture stress (Overend 2007). However, a direct relationship between crack velocity and crack branching was not available from experimental tests. A more recent hypothesis is that the branching stress is controlled by the strain energy release rate. The following relationship, called the crack branching equation, is an extension of Eq. (8), proposed for the failure stress vs. the mirror radius:

$$\sigma_f - \sigma_{ar} = \alpha r_m^{-1/2}, \quad (9)$$

Table 1 Parameters of the crack branching equation for annealed glass

	$\alpha$ [ $\text{Mpa m}^{1/2}$ ]	$\sigma_{ar}$ [ $\text{Mpa}$ ]
Mirror	1.98	9.6
Hackle	2.11	9.1
Branch	2.18	10.7

where  $\sigma_{ar}$  is interpreted as being an apparent residual compressive surface stress and  $\alpha$  is a constant value. Finally, the three branching constants  $\alpha_m$ ,  $\alpha_h$  and  $\alpha_b$ , as well as the corresponding apparent residual stress  $\sigma_{ar}$ , were determined in recent studies by Haldimann *et al.* (2010) and summarized in Table 1. Eq. (9) is valid for all points along the branching boundary.

The crack branching equation provides the failure stress, having measured the mirror radius  $r_m$ , the hackle radius  $r_h$  and the half branching length  $r_b$ . It is not always easy to apply because sometimes reading the fracture pattern becomes quite complex for the high stress values that produce the failure.

### 2.3 Strain energy in linear elastic solids

In a prismatic mono-dimensional structural element subjected to loads  $F_i$  acting in the plane containing the axis of symmetry of the cross section and the axis of the element, it is assumed that the transverse cross sections, which are perpendicular to the centroid axis, remain plane and perpendicular to the centroid axis of the beam. Indicating with  $V_i$  the displacement at the location and in the direction of the force, an increase in  $F_i$  gives a corresponding increase in the displacement, and consequently the work done by the load is

$$W_{ext} = \int_0^{V_i} F_i \cdot dv_i = \frac{1}{2} F_i \cdot V_i \quad (10)$$

In absence of any energy dissipation, this work is stored in the structure in the form of internal energy  $U_{int}$  done by the stress resultants in moving through the corresponding deformations; this is also called strain energy. For beams of span  $L$ , volume  $V$ , inertia bending moment  $I_x$  and material with elastic modulus  $E$ , the energy stored in the complete beam, subjected to a bending moment  $M_x$  and considering only the normal stress, may be obtained from Eq. (11)

$$U_{int} = \int_V \frac{\sigma_z^2}{2E} dV = \int_L \frac{M_x^2}{2E \cdot I_x} dz \quad (11)$$

In this context, thus we have  $W_{ext}=U_{int}$  because the work performed by the elastic body is completely transformed into elastic strain bending energy, which constitutes the internal energy of the beam. This balance between external work and internal work implies that the external forces are applied statically, i.e. in such a way that dynamic effects can be excluded which, due to damping, would cause a

dissipation of energy. Work and energy are expressed in the same units, the joule (J), which is equal to one Newton metre (N·m).

If experimental load-displacement diagrams are available that describe the mechanical behavior of the structures, the total work done by the applied loads can be evaluated measuring the area enclosed by the load-displacement curve.

#### 2.4 Statistical interpretation of brittle material strength

The statistical Weibull distribution is normally used to predict the strength of brittle materials, in which their intrinsic strength is sensible to material defectiveness. This distribution is based on the weakest-link-in-the-chain concept, in which the failure occurs when a part of material fails whose mechanical behavior is independent from that of the other parts of the material. The Weibull probability law is able to describe the variability of the strength of the material, and the failure risk  $dB$  is expressed in general as (Weibull 1939)

$$dB = -\log(1 - P_{f,0})dV \quad (12)$$

where  $P_{f,0}$  is the probability of failure of a small volume element  $dv$ .

The failure risk  $dB$  is a function of the stress  $\sigma$  and can be expressed by means of the characteristic function of the material  $n(\sigma) > 0$  which is a function of the applied stress

$$dB = n(\sigma)dv \quad (13)$$

and for a generic stress distribution the failure risk is

$$B = \int_V n(\sigma) dv \quad (14)$$

In those brittle materials in which fractures occur starting from the surface (e.g., with the defectiveness being due to the use and method of finishing), the volume integral can be replaced by a surface integral extended over the surface  $A$  of a layer of a small thickness and the failure risk can be expressed as

$$B = \int_A n(\sigma) da \quad (15)$$

Studies of Freudenthal (1968) showed how to correlate the flaw distribution to the Weibull distribution allowing to assert that the following characteristic function of the material  $n(\sigma)$  can be assumed

$$n(\sigma) = \left(\frac{\sigma}{\eta_0}\right)^m \quad (16)$$

defined in  $[0, +\infty)$  and where  $m$  and  $\eta_0$  are the shape and scale parameters, respectively. Assuming the material function in Eq. (16), the probability of failure of the two-parameter Weibull distribution is expressed as

$$P_{FAIL} = 1 - \exp\left[-\int_A \left(\frac{\sigma}{\eta_0}\right)^m da\right] \quad (17)$$

The 2PW distribution is considered a reliable statistical model for the strength characterization of brittle materials, and of glass in particular, and it is appreciated because its formulation is mathematically simple. The two parameters  $m$  and  $\eta_0$  cannot be measured directly, but are assessed for each group of samples. Indeed,  $m$  represents the data dispersion: the higher the  $m$  value, the lower the data dispersion, while  $\eta_0$  is considered the stress that corresponds to the 63% breakage probability. The cumulative probability of failure of this distribution is expressed by

$$F(\sigma) = 1 - \exp\left[-\left(\frac{\sigma}{\eta_0}\right)^m\right] \quad (18)$$

In the technical literature there are other kinds of Weibull distributions, such as the three-parameter distribution, in which the material function  $n(\sigma)$  is defined when  $\sigma \geq \sigma_0$  and  $\sigma_0$  is the third parameter that describes the lower bound of the strength. Han, Tang et al. (2009) suggest the use of the 3PW distribution for ceramic and high-strength glass. An accurate statistical interpretation of glass strength has been written by Pisano and Royer (2015) and an interesting review of the statistical distributions to be used to model the strength of float glass is in Ballarini *et al.* (2016).

### 3. Experimental procedure and results

In this experiment, five sets of small glass mono-dimensional elements having rectangular cross section were built using soda-lime silica float glass. The geometric characteristics, the edge finishing and the number of samples are indicated in Table 2. The specimens of sets A, B, C and D have the same cross section, while the length is greater for C and D. The set E samples have the biggest size. The five sets differed in their edge finishing, which was ground (further finishing after the cut) for sets A, C and E and simply cut (primary edge finishing) for sets B and D. The ratio between height ( $h$ ) and length ( $l$ ) of the elements in the various sets is almost constant, as is the ratio between the load span,  $s_l$ , and the support span,  $l_s$ . All specimens were furnished by the same manufacturers and were subjected to the same treatment (annealing) and working process (edge finishing) to obtain a similar level of surface defectiveness. A total of 107 specimens were tested.

#### 3.1 Bending tests

All the specimens were subjected to in-plane four-point bending tests in accordance with the UNI EN 1288-3 (2000) standard. Sets A, B, C and D were tested using a universal UTS testing machine (see Fig. 2(b)) following the test setup illustrated in Fig. 2(a). Due to their greater length, the set E specimens were tested following the same test setup and using another testing machine (with an electronic hydraulic jack for loading) capable of testing larger specimens than previous sets.

Table 2 Geometrical characteristics and edge finishing of glass elements and test stress rate

SET	b [mm]	h [mm]	l [mm]	Edge finishing	Number of samples	$l_s$ [mm]	$s_s$ [mm]	h/l	$s_s/l_s$	Stress rate [MPa/s]
A	8	50	400	Ground	25	360	120	0.12	0.33	0.59
B	8	50	400	Cut	25	360	120	0.12	0.33	0.59
C	8	50	550	Ground	19	500	160	0.09	0.32	0.85
D	8	50	550	Cut	18	500	160	0.09	0.32	0.87
E	8	100	1100	Ground	20	1000	300	0.09	0.30	0.73

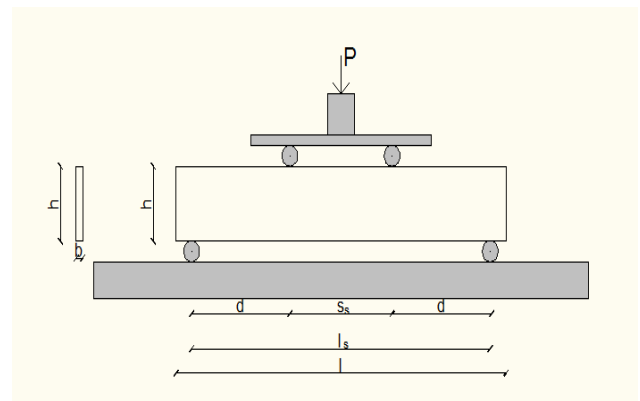
The specimens were equipped with LVDT (Linear Variable Displacement Transformer) inductive transducers in order to record the vertical displacement (Loktinov 2016). The load was statically applied at a stress rate of 0.75 MPa/s  $\pm$  0.15 MPa/s until the collapse. The laboratory temperature was 22°C and the relative humidity was 44%. Testing conditions were within the limits of standard recommendations for four-point bending tests [EN 1288-3, 2000], i.e., in the range of 23 $\pm$ 5°C for temperature and 40-70% for relative humidity. The failure load  $P_f$ , the time at failure  $t_f$  and the maximum displacement in the midspan  $w_f$  [mm] were automatically recorded by a data acquisition system.

The mean results for each set are shown in Table 3. As a first result of the bending tests, it can be observed that the mean failure load  $P_f$  of the set A is greater than that of set B. In set C and D, the  $P_f$  for the set of cut edge beams is slightly smaller than for the ground edge beams. The failure occurred always inside the load span: cracks spread from the tensile edge towards the compressed edge with several branchings. The load displacement diagram of each tests showed linear behavior from zero to limit load (see Fig. 3). Once  $P_f$  was known, the bending moments of each specimen were calculated at the failure and the failure stress  $f$  was computed by means of the following equation

$$f = \frac{\left(\frac{P_f}{2}\right)d}{b \frac{h^2}{6}} = \frac{3P_f d}{bh^2}, \quad (19)$$

where  $d$  [mm] is the distance between the load point and the support, and  $b$  [mm] and  $h$  [mm] are the width and the height of the cross section, respectively. It is obvious that bending tests generated variable tensile stress that is maximum at the intrados of the specimen and decrease towards the compressed area. Table 3 also gives the vertical displacement measured in the midspan at failure. In addition, the last two columns of this table show the energy values: the first is the elastic strain energy released upon initial failure and evaluated by measuring the area closed from the load-displacement curve in the experimental bending diagram; the second is the external work computed with reference to the failure values of the load and the displacement.

During testing, it was observed that there were significant differences in the failure mode among the specimens. Specimens that reached a high load showed more cracks than specimens that failed at a low load. Branched cracking patterns occurred in specimens in which more elastic energy was stored. The set A specimens showed multiple fracture branches compared to the B set specimens, which supported lower loads. In this regard, it is pointed out that the set A specimens supplied greater strength and energy than the set B specimens.



(a)



(b)

Fig. 2 Test set-up used for in-plane four point bending

Table 3 Mean values at failure for each set

SET	Experimental values						Theoretical values
	$P_f$ [N]	$t_f$ [s]	$M_f$ [Nmm]	$f$ [Mpa]	$w_f$ [mm]	$E$ [J]	$E$ [J]
A	2290.14	75.54	148859	41.22	2.52	2.9	2.9
B	1864.60	66.56	121199	33.56	2.22	2.1	2.1
C	1741.98	51.10	148067	42.81	2.12	1.8	1.8
D	1710.18	49.85	145365	41.26	1.66	1.5	1.5
E	3446.28	59.88	603098	40.82	2.00	5.3	4.8

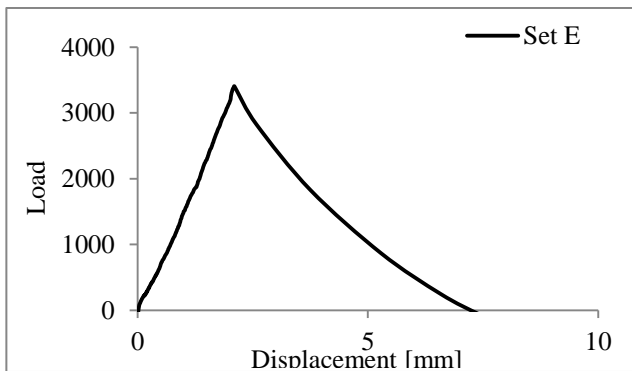


Fig. 3 Load-displacement diagram type

### 3.2 Analysis of the specimens fracture

#### 3.2.1 Fracture analysis

Given that the specimens were tested in flexure, each of them failed at the intrados of the glass element in mode I, which is normal-opening according to linear elastic fracture mechanics (LEFM) theory, i.e., subjected to tensile stress perpendicular to the crack plane. After the failure of the glass elements, the fractured section of each specimen was examined according the ASTM C1678 (2010) standard, using an optical microscope with polarized light, Hund mod. H600. Important information was collected on flaw sizes, fracture origin and fracture mirror sizes. Fig. 4 shows some significant microscope images of the fracture surface. Fig. 4(a) shows the intrados of the beam with beveled edges and the way to identify the flaw and the mirror zone. Figs. 4(b) and 4(c) are the microscope images of the fractures in which is easy to spot the origin of the fracture (white stain on the edge of the glass beam). The first image shows the whole fracture surface, and the fracture mirror zone can clearly be seen to be semi-circular, being of surface origin in tensile specimens. The second image (see Fig. 4(c)) shows a fracture mirror that is a quarter circle, since this forms from a corner origin. The mirror boundary is partial, probably because the crack did not achieve sufficient velocity within the edges of the specimen. Furthermore, separate mirror, mist and hackle regions and the apparent boundaries between them can be identified. Each has a corresponding mirror constant according Eq. (8). The mirror-mist boundary is most commonly referred to as the inner mirror boundary, and its mirror constant is determined.

The failure strength  $\sigma_f(t_f)$  has been calculated for each sample using Eq. (6), knowing the flaw depth  $a$ , the time at failure  $t_f$  and the critical value of  $K_{Ic}$ . In this analysis it was assumed that the flaw depth  $a$  does not change during loading. The values of  $v_0$  and  $n$  are assumed to be 0.01 mm/s (for laboratory condition) and 16, respectively. The geometric factor  $Y$  assumes a constant value for each edge crack configuration. This value was chosen by Haldimann (2006) observing each crack pattern (e.g.,  $Y$  is 0.722 for a quarter-circle crack on glass edges, and is 1.12 for a long, straight-fronted plane edge crack in a semi-infinite specimen).

The results of the post-fracture analysis are summarized in Table 4 for each set. The table shows the results of the microscopic analysis in the first three columns on the left: i.e., the mean values of the mirror radius  $r_m$  and the flaw depth  $a$ , microscopically measured, and the mean value of the ratio  $r_m/a$ . It is possible to observe that the ratio between the mirror radius  $r_m$  and the flaw depth  $a$  is almost constant in the 9-10 range.

The three columns on the right in Table 4 give the mean values of the time reference  $t_{ref}$  (derived from Eq. (7)), the strength  $\sigma_f(t_f)$  and the inert strength  $\sigma_f(t_{ref})$  (both calculated using Eq. (6) knowing the flaw depth  $a$ , the time failure and the critical value of  $K_{Ic}$ ). Stress at the failure time  $t_f$  takes into account the effect of the stress corrosion, due to the duration of loading (Table 3) in which humidity and temperature produce a decrease in the strength of the glass, causing a subcritical growth of the flaw. If the loading duration is very short, the effect of the stress corrosion could be neglected, and the strength of the glass corresponds to the inert strength.

Table 4 Mean values of the microscopic analysis and of the strength

SET	Mean values of the microscopic analysis			Mean values of the strength		
	$r_m$ [mm]	$a$ [ $\mu$ m]	$r_m/a$	$\sigma_f(t_f)$ [MPa]	$t_{ref}$ [s]	$\sigma_f(t_{ref})$ [MPa]
A	2.50	292.4	9.0	52.91	4.18	54.03
B	3.89	456.1	9.3	45.43	6.52	46.50
C	2.14	324.5	10.3	52.34	4.64	52.09
D	2.46	258.4	9.6	48.10	3.69	48.12
E	2.56	271.5	10.0	55.01	3.88	54.91

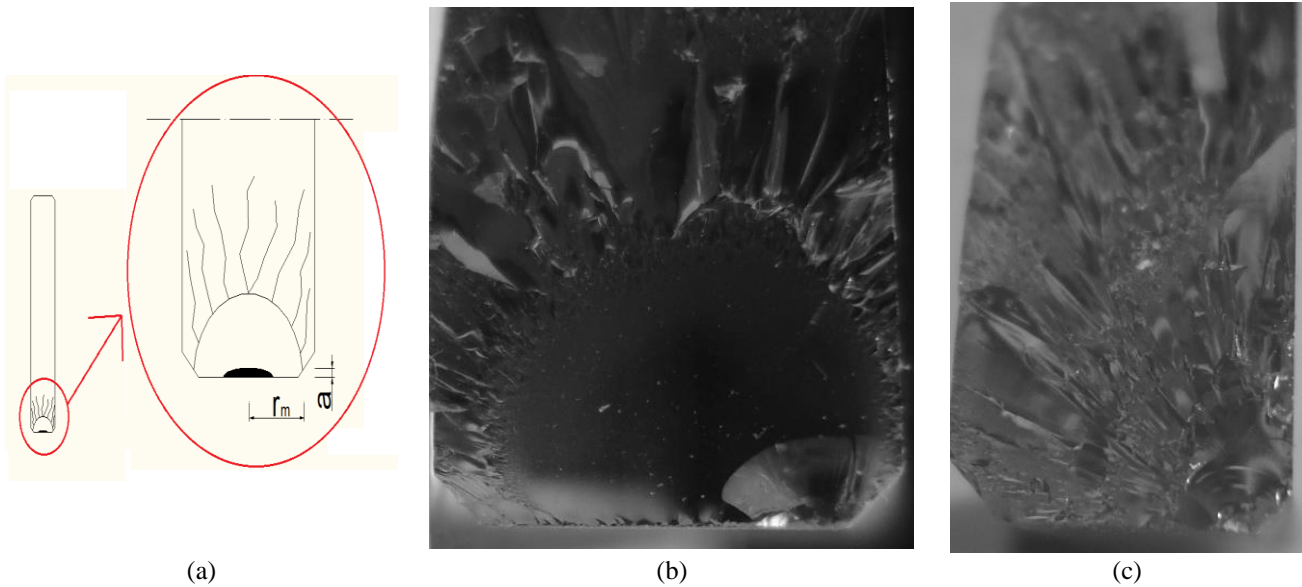


Fig. 4 (a) scheme of the fracture mirror, (b) and (c) microscope images of the fracture mirrors

### 3.2.2 Statistical analysis

Glass strength was analyzed by a statistical study using the two-parameter Weibull distribution fitting the failure stress data. The shape parameter  $m$  and the scale parameter  $\eta_0$  were calculated through a regression of the data adopting the least-square method for each set (Table 5).

The diagram in Fig. 5 shows the cumulative probability function for each set, and the minimum, maximum and mean values of the failure strength  $\sigma_f(t_f)$  are given in Table 6. The stress values vary from 16.24 MPa to 97.35 MPa, while the mean stress values vary from 45.43 MPa to 55.01 MPa.

Table 5 Values of the parameter  $\eta_0$  and  $m$  of the 2PW distribution

SET	$m$	$\eta_0$
A	4.16	59.55
B	9.24	48.01
C	4.84	55.16
D	2.49	68.99
E	3.17	63.73

Table 6 Mean, maximum and minimum strength of each distribution

SET	$\sigma_f(t_f)$ [Mpa]	$\sigma_f(t_f)_{MIN}$ [Mpa]	$\sigma_f(t_f)_{MAX}$ [Mpa]	Standard deviation
A	52.91	40.45	91.82	11.93
B	45.43	35.49	57.41	5.48
C	52.34	16.24	74.28	12.54
D	48.10	37.62	67.23	7.22
E	55.01	37.87	97.35	16.43

Variations were observed between different edge finishes: standard deviation values of the sets considered vary in the range of 5.5-16.4. Observing the standard deviation values, it can be noted that sets A, C and E with ground finishing are subject to a greater dispersion of stress values compared to sets B and D, whose edges have been simply cut. On the contrary, the latter show values lower than the average stress compared to the specimens with a ground finish.

## 4. Analysis of the results and discussion

As regards the tests performed, the experimental results were compared with the LEFM theory, and the glass strength was analyzed with a statistical study using the two-parameter Weibull distribution that best fit the failure stress data.

### 4.1 Analysis of the fracture surface

In order to compare the LEFM theory and the fracture surface analysis, the parameters for the crack branching equation,  $\alpha$  and  $\sigma_{ar}$ , were determined by a linear regression in the diagram of the failure stress and the mirror length (see Fig. 6). The mirror lengths were measured together with the flaw depth in the post failure microscopic analysis, and were used to assess the branching constants in the branching equation.

For each set it was possible to plot the strength  $\sigma_f$  versus the measured mirror length  $r_m(m)^{1/2}$ , as for set A in Fig. 6. The best-fit straight line of the plotted points represents the equation branching line where  $\alpha$  is the slope of the line and  $\sigma_{ar}$  is the failure stress-intercept. In all the sets,  $\sigma_{ar}$  was a non-zero value; this was due to the presence of a compressive surface residual stress. Like with the other sets, parameters  $\alpha$  and  $\sigma_{ar}$  obtained with a linear regression in

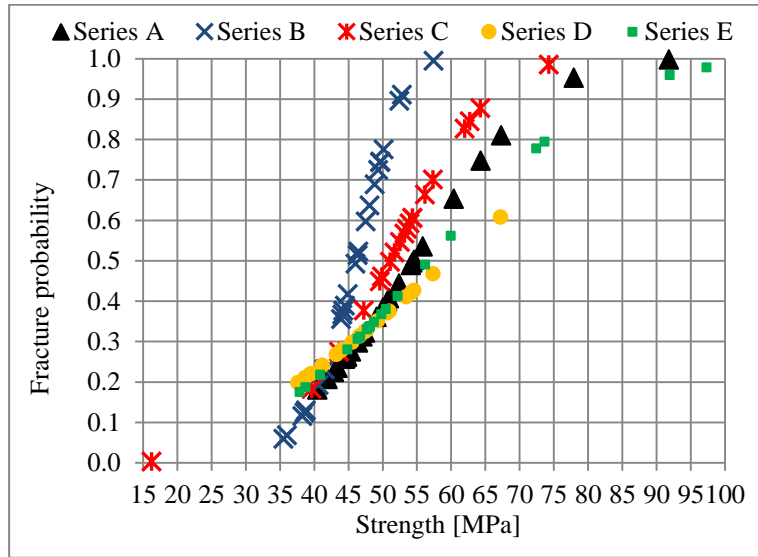


Fig. 5 Cumulative probability function for each set

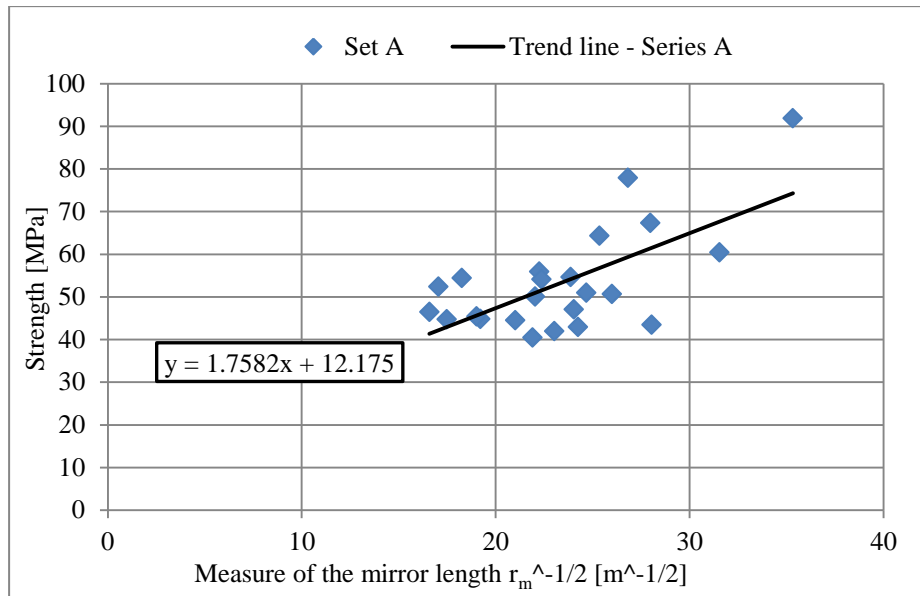


Fig. 6 Diagram of set A: the strength  $\sigma_f(t_f)$  vs. the mirror length  $(r_m \text{ (m)})^{-1/2}$

Table 7 Parameters of the crack branching equation

SET	$\alpha$	$\sigma_{ar}$
A	1.76	12.18
B	1.43	13.71
C	1.96	13.42
D	1.66	13.23
E	1.88	11.63

accordance with the crack branching equation are shown in Table 7. The measured values are in accordance with those proposed in the literature. The obtained values of  $\sigma_{ar}$  are slightly higher than those proposed in Table 1 by Overend *et al.* (2007), while the values of  $\alpha$  are a little bit lower. The

values are similar for all sets of samples. The differences could be caused by the dispersion of the failure strength values measured on the glass beams.

#### 4.2 Linear Elastic Fracture Mechanics – LEFM

As explained by this theory, in general the inert strength  $\sigma_f(t_{ref})$  is greater than the strength  $\sigma_f(t_f)$  where stress corrosion is considered. The results of this study given in Table 4 confirm this trend. These differences are little because the loading durations is small. The stress corrosion law was obtained from the mean values of each set of beams and was plotted in a strength-loading duration diagram, in which the values of the mean strength for each lot of specimens are also drawn (see Fig. 7). Each curve

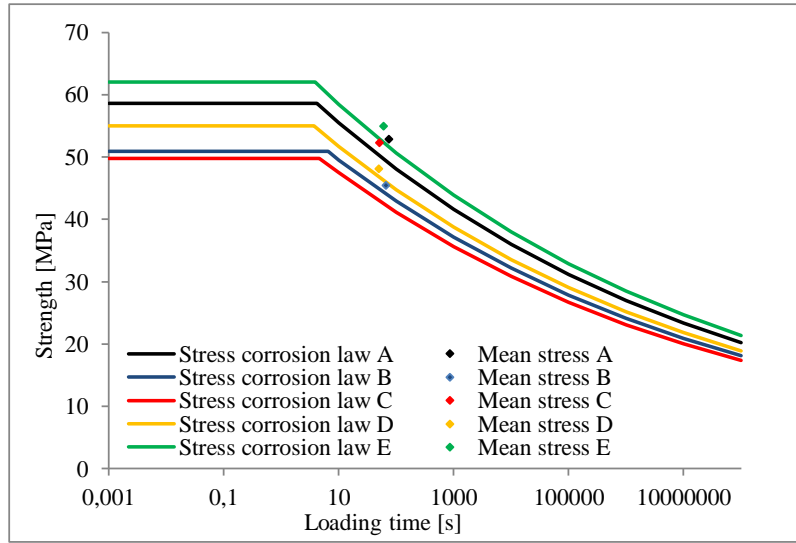


Fig. 7 Stress-corrosion law for each set of specimens

Table 8 Mean values of the strength from fracture surface analysis (FSA), strength  $\sigma_f(t_f)$  and inert strength  $\sigma_f(t_{ref})$  from LEFM

SET	$\sigma_f$ [MPa] FSA	$\sigma_f(t_f)$ [MPa] LEFM	$\sigma_f(t_{ref})$ [MPa] LEFM
A	54.00	52.91	54.03
B	45.42	45.43	46.50
C	53.86	52.34	52.09
D	51.81	48.10	48.12
E	50.78	55.01	54.91

consists of two lines: the horizontal one that represents the level of inert strength and another line that identifies the time-dependent strength. This diagram confirms that the time-dependent strength is smaller than the inert strength.

The crack branching equation (Eq. (9)) makes it possible to compute  $\sigma_f$ , knowing  $\alpha$ ,  $\sigma_{cr}$  and  $r_m$ . The strength values,  $\sigma_f$ , are summarized in Table 8, together with the strengths  $\sigma_f(t_f)$  and  $\sigma_f(t_{ref})$  obtained from LEFM. The decrease in  $\sigma_f(t_f)$  computed by LEFM was estimated at 2% to 7% compared to  $\sigma_f$  calculated by the fracture surface analysis, for all the specimens.

#### 4.3 Energy release

During the four point bending tests it was observed that there were significant differences among the specimens in the breaking mode. Specimens that reached a high load showed more cracks than specimens that failed under a lesser load. A branched cracking pattern occurred in specimens in which more elastic energy was stored. For example, the set A specimens showed multiple fracture branches compared to the set B specimens, which supported lesser loads. In this respect, it is emphasized that set A specimens supplied greater strength and energy than set B specimens. These findings confirm that the failure mode

depends on the amount of elastic energy stored before failure and, consequently, on the elastic strain energy release. These results are in accordance with experiments on other brittle materials and also in hybrid structures as for example in glass reinforced with tensile resistant materials (Corradi and Speranzini 2019).

#### 4.4 Size effect

Due to the size effect, the dimension of the loading area has an influence on the failure stress. Indeed, an increase in the dimension of a structural element causes a decrease of the strength. This effect can be explained with the Weibull theory referring to the fact that a larger panel is more likely to have a large flaw in a high stress region than small panel. Weibull effective volumes and surfaces can be used to scale brittle materials strengths from one component size to another or from one loading configuration to another, as explained in Quinn 2003. Davies (1973) and Fisher *et al.* (2002) proposed a model based on the effective volume  $V_{eff}$  or effective surface  $S_{eff}$  to obtain a strength which is independent of both structural element size and the load configuration that causes the breakage. The size effect is given as

$$\frac{\sigma_1}{\sigma_2} = \left( \frac{V_{eff.2}}{V_{eff.1}} \right)^{\frac{1}{m}}, \quad (20a)$$

$$\frac{\sigma_1}{\sigma_2} = \left( \frac{S_{eff.2}}{S_{eff.1}} \right)^{\frac{1}{\beta}}, \quad (20b)$$

where  $\sigma_1$  and  $\sigma_2$  are the strength for two elements of different sizes.  $V_{eff.1}$  and  $V_{eff.2}$  are the respective statistical size of the volumes which are effectively subjected to tensile stress and  $m$  is the Weibull modulus of the set

Table 9 Mean values of Weibull shape parameter, strength, effective volume and geometrical dimensions, for each set

SET	b [mm]	h [mm]	$l_s$ [mm]	m	$\sigma_r(t_f)$ [MPa]	$V_{\text{eff}}$ [mm <sup>3</sup> ]
A	7.95	50.38	360	4.16	52.91	66675
B	7.84	50.45	360	9.24	45.43	56745
C	7.85	51.08	500	4.84	50.74	89706
D	7.83	51.87	500	2.49	50.14	106490
E	7.94	105.05	1000	3.17	55.01	411538

Table 10 Size effect analysis (effective volume and surface) for each set

	$\sigma_B/\sigma_D$	$\sigma_A/\sigma_C$	$\sigma_A/\sigma_E$	$\sigma_C/\sigma_E$
Stress ratio	0.91	1.04	0.96	0.92
	$(V_{\text{eff},D}/V_{\text{eff},B})^{1/m}$	$(V_{\text{eff},C}/V_{\text{eff},A})^{1/m}$	$(V_{\text{eff},E}/V_{\text{eff},A})^{1/m}$	$(V_{\text{eff},E}/V_{\text{eff},C})^{1/m}$
Effective volume ratio	1.11	1.06	1.54	1.37
	$\sigma_B'/\sigma_D'$	$\sigma_A'/\sigma_C'$	$\sigma_A'/\sigma_E'$	$\sigma_C'/\sigma_E'$
Stress ratio	0.91	1.04	0.96	0.92
	$(S_{\text{eff},D}/S_{\text{eff},B})^{1/\beta}$	$(S_{\text{eff},C}/S_{\text{eff},A})^{1/\beta}$	$(S_{\text{eff},E}/S_{\text{eff},A})^{1/\beta}$	$(S_{\text{eff},E}/S_{\text{eff},C})^{1/\beta}$
Effective surface ratio	1.00	1.08	1.24	1.12

defining the population of the volume defects (Eq. 20(a)). To use this relationship, a unimodal flaw population related to the volume and a Weibull two-parameter distribution must be assumed. If the surface defects are responsible for the failure the size effect is expressed by (Eq. 20(b)), in which  $S_{\text{eff}}$  replaces  $V_{\text{eff}}$  and  $\beta$  is the Weibull modulus of the set defining the population of the surface defects.

For the four-point bending tests executed, the strength and the geometrical dimensions are taken into account to verify the relation (20a) and are summarized in Table 9. It should be noted that the low Weibull modulus of the investigated glass material lowers the reliability of the strength results because of the large scatter of the strength values, as in sets D and E. These are usual values for glass material.

The results obtained with Eq. (20) are shown in Table 10. Consider sets A and C (ground edge specimens) for the analysis on the size effect. The value  $\sigma_f(t_f)$  of set A is higher than that of set C, while the effective volume of A is lower than that of set C. In this case, smaller samples show higher stress, which is what we expect from the theory, and the results are in accordance with (Eq. 20(a)). The results from ratios  $\sigma_A/\sigma_E$  and  $\sigma_C/\sigma_E$  are not equal to the corresponding  $(V_{\text{eff},E}/V_{\text{eff},A})^{1/m}$  and  $(V_{\text{eff},E}/V_{\text{eff},C})^{1/m}$ .

If instead the analysis is performed in terms of effective surface  $S_{\text{eff}}$ , the results (Table 10) show effective surfaces ratios closer to those of the stress ratio. In this case, the surface size effect characterizes the defect population of the specimen better than the volume size effect.

## 5. Conclusions

In this work the relationship between flaws, cracks and strength in brittle materials subjected to tensile stress was

analyzed by means of observations and measurements of the cracks after the collapse. The flaws cause stress concentrations that may lead to underestimation or overestimation of strength, and for this reason the tensile strength of brittle materials cannot be considered a material constant. An accurate approach requires knowledge of fracture mechanics properties such as fracture toughness and slow crack growth, which are able to account for flaws and stress concentrations.

This study starts from the results of 107 specimens subjected to in-plane four point bending tests. To this end it was decided to use specimens of annealed float glass because the results were expected to be more significant than with other brittle materials. The specimen sets differed from one another by size and edge finishing. All the specimens failed at the intrados of the glass element in mode I, which is normal-opening according to LFM theory. The structural response was studied in terms of failure loads and dissipated energy. During testing, it was observed that there were significant differences in the failure mode among the specimens. Specimens that reached a high load showed more cracks than specimens that failed at a low load. Branched cracking patterns occurred in specimens in which more elastic energy was stored. For example specimens with ground edges showed multiple fracture branches compared to specimens with simply cut edges, which supported lower loads.

The fracture surface of the specimen fragments was analyzed by means of a fractographic examination, obtaining quantitative information about the loading condition, fracture origin and flaw size. Failure stress can be computed after having measured the mirror radius  $r_m$ , the hackle radius  $r_h$  and the half branching length  $r_b$ . The analysis and measurements performed show the relation

between flaw size and glass strength and confirms that the larger is the critical flaw at the beginning of the failure, the lower is the strength. An equivalent relation was found for the mirror radius: the larger the mirror radius, the lower the strength. Failure stress was higher for glass specimens having ground edge finishing than those simply cut; indeed, this glass edge processing reduces the maximum depth of the flaw and increases the strength.

For each specimen, the values for inert strength and time dependent strength, taking into account the effect of the stress corrosion due to the duration of loading, were computed using the LEFM formulations, knowing the parameters measured on the crack plane.

Lastly, the experimental data agreed with the theoretical results obtained from the fracture mechanics analysis. Size effect analysis shows that the surface size effect characterizes the defect population of the glass specimen better than the volume size effect. Furthermore, the results of this study show the applicability of Weibull statistics to explain the differences in the results of 4-point bending tests when different sizes are used.

Therefore, this survey proves the possibility of determining the stress of brittle materials at the time of breaking directly on the fragments by means of analyses and measurements performed on the plane containing the fracture surface.

## References

- Akbarov, S.D., Cafarova, F.I. and Yahnioğlu, N. (2018), "The influence of initial stresses on energy release rate and total electro-mechanical potential energy for penny-shaped interface cracks in PZT/Elastic/PZT sandwich circular plate-disc", *Smart Struct. Syst.*, **22**(3), 259-276. DOI: 10.12989/sss.2018.22.3.259
- Andreozzi, L., Briccoli Bati, S., Ranocchiai, G. and Zulli, F. (2015), "Weathering action on thermo-viscoelastic properties of polymer interlayers for laminated glass", *Constr. Build. Mater.*, **98**, 757-766.
- ASTM C1678-10 (2010), *Standard practice for fractographic analysis of fracture mirror sizes in ceramics and glasses*, American Society for Testing materials.
- Ballarini, R., Pisano, G. and Royer-Carfagni, G. (2016), "The lower bound for glass strength and its interpretation with generalized Weibull statistics for structural application", *J. Eng. Mech.*, **142**(12), 1-20.
- Brenchich, A. and Gambarotta, L. (2001), "Isotropic damage model with different tensile-compressive response for brittle materials", *Int. J. Solids Struct.*, **38**(34-35), 5865-5892.
- Briccoli Bati, S., Ranocchiai, G., Reale, C. and Rovero, L. (2010), "Time-dependent behavior of laminated glass", *J. Mater. Civ. Eng.*, **22**, 389-396.
- Carpinteri, A. (1992), *Meccanica dei Materiali e della Frattura*, Pitagora Editrice, Bologna, Italy.
- Castilone, R.J., Glaesemann, G.S. and Hanson, T.A. (2002), "Relationship between mirror dimensions and failure stress for optical fibers", *Proc. SPIE 4639, Optical Fiber and Fiber Component Mechanical Reliability and Testing II*, (Eds., M.J. Matthewson and C.R. Kurkjian), 11-20.
- Castori G. and Speranzini, E. (2017), "Structural analysis of failure behavior of laminated glass", *Compos. B Eng.*, **125**, 89-99. DOI: 10.1016/j.compositesb.2017.05.062
- Cervera, M., Tesei, C. and Ventura, G. (2018), "Cracking of quasi-brittle structures under monotonic and cyclic loadings: a d+/d-damage model with stiffness recovery in shear", *Int. J. Solid Struct.*, **135**, 148-171.
- Charler, R. (1958), "Static fatigue of glass I", *J. Appl. Phys.*, **29**(11), 1549-1553.
- Charler, R. (1958), "Static fatigue of glass II", *J. Appl. Phys.*, **29**(11), 1554-1559.
- Ciccotti, M. (2009), "Stress-corrosion mechanism in silicate glasses", *J. Phys. D: Appl. Phys.*, **42**, 1-29.
- Collini, L. and Royer, C.G. (2014), "Flexural Strength of glass-ceramic for structural application", *J. Eur. Ceram. Soc.*, **34**, 2675-2685.
- Congleton, J. and Petch, N.J. (1967), "Crack branching", *Philos. Mag.*, **16**(142), 749-760.
- Corradi, M. and Speranzini E. (2019), "Post-cracking capacity of glass beams reinforced with steel fibers", *Materials MDPI*, **12**(2), 231-246. DOI:10.3390/ma12020231
- Davies, D. (1973), "A statistic approach to engineering design in ceramics", *Proc. Br. Ceram Soc.*, **22**, 429-452.
- EN 1288-3, (2000), Glass in building - Determination of the bending strength of glass - Part 3: Test with specimen supported at two points (four point bending), European Standard.
- Fischer, H., Rentzsch, W. and Marx, R., (2002), "A modified size effect model for brittle non-metallic materials", *Eng. Fract. Mech.*, **69**, 781-791.
- Foraboschi, P. (2009), "Buckling of a laminated glass column under test", *Struct. Eng.*, **87**(1), 2-8.
- Foraboschi, P. (2017), "Analytical modeling to predict thermal shock failure and maximum temperature gradients of a glass panel", *Mater Des.*, **134**, 301-319.
- Freudenthal, AM. (1968), "Statistical approach to brittle fracture", (Ed., H. Liebowitz), *Fracture, an advanced treatise*, II, Academic Press, New York, 591-619.
- Griffith, A.A. (1920), "The phenomena of rupture and flaw in solid", *Philos. T. R. Soc. London*, **221**, 163-198.
- Haldimann, M. (2006), "Fracture strength of structural glass elements – analytical and numerical modelling, testing and design", PhD Dissertation n. 3671, EPFL, Lausanne, Switzerland.
- Haldimann, M., Luibe, A. and Overend, M. (2010), "Structural use of glass", *Struct Eng, Documents, IABSE - AIPC – IVBH 10*.
- Han, Z., Tang, L., Xu, J. and Li, Y. (2009), "A three-parameter Weibull statistical analysis of the strength variation of bulk metallic glasses", *Scripta Mater.*, **61**, 923-926.
- Inglis, C.E. (1913), "Stresses in a plate due to the presence of cracks and sharp corners", *T. Inst. Naval Arch.*, **55**, 219-230.
- Irwin, G.R. (1957), "Analysis of stresses and strains near the end of a crack traversing a plate", *J. Appl. Mech.*, **24**, 361-364.
- Jang, K. and An, Y.K. (2018), "Multiple crack evaluation on concrete using a line laser thermography scanning system", *Smart Struct. Syst.*, **22**(2), 201-207. DOI: 10.12989/sss.2018.22.2.201
- Johnson, J.W. and Holloway, D.G. (1966), "Shape and size of fracture zones on glass fracture surfaces", *Philos. Mag.*, **148**(30), 731-43.
- Kim, B. and Cho, S. (2018), "Efflorescence assessment using hyperspectral imaging for concrete structures", *Smart Struct. Syst.*, **22**(2), 209-221. DOI: 10.12989/sss.2018.22.2.209
- Levengood, W.C. (1958), "Effects of original flaw Characteristics on Glass Strength", *J. Appl. Phys.*, **29**(5), 820-26.
- Loktionov, A.P. (2016), "A measuring system for determination of a cantilever beam support moment", *Smart Struct. Syst.*, **19**(4), 431-439. DOI : 10.12989/sss.2017.19.4.431
- Marsili, R., Rossi, G. and Speranzini, E. (2017), "Causes of uncertainty in thermoelasticity measurements of structural

- elements”, *Smart Struct. Syst.*, **20**(5), 539-548, DOI: 10.12989/sss.2017.20.5.539.
- Overend, M., De Gaetano, S. and Haldimann, M. (2007), “Diagnostic Interpretation of Glass Failure”, *Struct. Eng.*, **2**, 151-158.
- Pisano, G. and Royer, C.G. (2015), “The statistical interpretation of the strength of float glass for structural applications”, *Constr. Build. Mater.*, **98**, 741-756.
- Quinn, G. D. (2003), “Weibull effective volumes and surfaces for cylindrical rods loaded in flexure”, *J. Am. Ceram. Soc.*, **86**(3): 475-479.
- Quinn, G., Swab, J.J. and Slavin, M.J. (1990), “A proposed standard practice for fractography analysis of monolithic advanced ceramics”, US Army Materials Technology Laboratory.
- Turco, E. and Rizzi, N.L. (2016), “Pantographic structures presenting statistically distributed defects: Numerical investigations of the effects on deformation fields”, *Mech. Res. Commun.*, **77**, 65-69.
- Weibull, W. (1939), “A statistical theory of the strength of materials”, *Ingeniorsvetenskapsakademiens Handlingar*, **151**, 1-45.
- Wiederhorn, S.M. (1969), “Fracture surface energy of glass”, *J. Am. Ceram. Soc.*, **52**, 99-105.
- Wiederhorn, S.M. and Bolz, L.H. (1970), “Stress-corrosion and static fatigue of glass”, *J. Am. Ceram. Soc.*, **53**(10), 543-548.
- Wiederhorn, S.M. and Evans, A.G. (1974), “Proof testing of ceramic materials – an analytical basis for failure prediction”, *Int. J. Fracture*, **10**(3), 379-392.